Supporting Information

Atomically Anchored Cu on MXene-Derived TiO_2/Ti_3C_2 Enables Cu–Ti Dual Sites for Selective Urea Photosynthesis from CO_2 and Nitrate

*Zengxin Lou[a] , Kai Kang[a] , Pingping Zhang[b], Qi Zhong[a] , Yong Liu[a], Kaiqiang Liu[a] , Wenzhuo Yuan[a] , Juan Liu[a], Yongchao Bao[a]**

a College of Environmental and Safety Engineering, Qingdao University of Science and Technology, Qingdao 266042, P. R. China

b College of Materials Science and Engineering, Qingdao University of Science and Technology, Qingdao 266042, P. R. China

**Corresponding author: yuzhong3688@163.com (Yongchao Bao)*

S1. Experimental Section

S1.1 Reagents

Hydrochloric acid (HCl), lithium fluoride (LiF), and ethanol, all of analytical grade, were procured from Sinopharm Chemical Reagent Co. Titanium aluminum carbide (Ti_3AlC_2) was obtained from Beijing Beike New Material Technology Co. Potassium nitrate (KNO_3, 99%), urea (CH_4N_2O, 99.99%), and copper nitrate trihydrate ($Cu(NO_3)_2·3H_2O$) were purchased from Shanghai Aladdin Biochemical Science and Technology Co. Furthermore, potassium bicarbonate ($KHCO_3$, 99.5%) and thiourea (CH_4N_2S, 99%) were sourced from Shanghai McLean Biochemical Co., Ltd.

S1.2 Preparation of Ti_3C_2

Ti_3C_2 was synthesized by etching Al in LiF, using Ti_3AlC_2 as the precursor, according to previously reported methods [1,2]. Initially, 2.0 g of LiF was added to a plastic flask containing 40 mL of 6 M hydrochloric acid solution and stirred for 10 minutes. Subsequently, 1 g of Ti_3AlC_2 was gradually introduced, and the mixture was stirred for 48 hours in a water bath at 35 °C. The solution was then centrifuged at 8,000 rpm to wash the product until the pH reached neutrality. The resulting material was transferred to an iodine volumetric flask, and deionized water was added to a final volume of approximately 150 mL. To this, 10 mL of dimethyl sulfoxide (DMSO) was added, and nitrogen gas was introduced. The solution was aerated for 30 minutes to remove oxygen and then stirred for 24 hours at room temperature at medium speed. The suspension was subsequently washed twice by centrifugation with ethanol and three times with deionized water at 8,000 rpm, then transferred to an iodine volumetric flask. Deionized water was again added to achieve a final volume of about 150 mL. Nitrogen aeration continued for 30 minutes, followed by ultrasonication for 6-8 hours. The suspension was then centrifuged at 8,000 rpm for 15 minutes to retain the product. The resulting suspension, a typical 2D ultrathin Ti_3C_2 suspension, is stored at low temperature under a nitrogen atmosphere.

S1.3 Determination of Optimal Preparation Conditions for TiO_2/Ti_3C_2 with the Highest Catalytic Performance

TiO_2/Ti_3C_2 series samples were synthesized by solvothermal method. As the solvothermal temperature and duration increased, the MXene sheets became progressively covered with TiO_2 aggregates. This increase in specific surface area provides more active sites and shortens the charge migration distance, likely suppressing the recombination of photogenerated electron–hole pairs [3]. The urea yields of all samples (TT1–TT9) are summarized in Table S1 and visualized in a three-dimensional surface plot (Figure S1). Analysis reveals that the carbon–nitrogen coupling efficiency improved with higher synthesis temperatures; however, the urea yield did not increase monotonically with prolonged reaction time. When the duration was extended to 24 hours, the yields were generally lower than those obtained at 15

hours, likely due to over-oxidation leading to etching and structural degradation of the Ti_3C_2 MXene framework, compromising its role as an electron acceptor [4]. Among all nine conditions, sample TT8 (synthesized at 220 °C for 15 hours) demonstrated the highest carbon–nitrogen coupling performance, achieving a urea production rate of 5.26 $\mu mol \cdot h^{-1} \cdot gcat^{-1}$ under simulated solar irradiation. Furthermore, copper was introduced into the optimal TT material via impregnation with different loadings.

S1.4 Preparation of Cu/Ti_3C_2 material

Cu/Ti_3C_2 composites were synthesized following the methodology described by Liu et al.[5]. Initially, 100 mg of synthesized Ti_3C_2 was dispersed in 20 mL of ethylene glycol and stirred for 2 hours at room temperature. Subsequently, 1.91 mg of $Cu(NO_3)_2 \cdot 3H_2O$ was added to the dispersion, and the mixture was stirred for an additional 12 hours, the resultant product was centrifuged and washed two to three times with deionized water. The final product, with a theoretical Cu loading of 0.5 wt%, was obtained after vacuum drying at 60 °C for 12 hours. The corresponding XRD patterns are shown in Figure S2.

S1.5 Preparation of Cu/TiO_2 material

TiO_2 was prepared as a supported catalyst via hydrothermal synthesis [6]. A homogeneous mixture was formed by adding 3 mL HF dropwise to 25 mL tetrabutyl titanate with stirring. This mixture was heated in a Teflon-lined autoclave at 180 °C for 24 h. The resulting precipitate was washed with deionized water and ethanol, then treated with 0.1 M NaOH aqueous solution under stirring for 7 h to remove fluoride residues, yielding pure TiO_2 nanosheets.

Based on the precipitation method described in the literature [7], atomically dispersed Cu species anchored on TiO_2 nanosheets were prepared. Specifically, 40 mg of as-prepared TiO_2 nanosheets were dispersed in 40 mL of NaOH aqueous solution (0.25 M). At room temperature, 410 μL of $Cu(NO_3)_2$ aqueous solution (0.0077 M) was added under stirring. After stirring for 6 h, the precipitate was washed repeatedly with deionized water until the pH of the solution reached 7. Finally, the washed precipitate

was dried at 353 K for 12 h to obtain the atomically dispersed Cu-anchored TiO_2 catalyst with a Cu loading of 0.5 wt%.

S1.6 Determination of NH_3

The indophenol blue method was utilized for the specific and low-toxicity detection of ammonia [8]. Under alkaline conditions (sodium hydroxide), ammonia reacts with salicylic acid and sodium hypochlorite, catalyzed by sodium nitroferricyanide, to form a blue-green chromophore with a characteristic absorption at 650 nm. The reagent solutions were prepared as follows: Solution A (5 wt% salicylic acid and 5 wt% disodium citrate dihydrate in 2.0 M NaOH), Solution B (0.05 M NaOCl), Solution C (1 wt% sodium nitroferricyanide), and Solution D (1 wt% EDTA disodium salt). The assay was conducted by sequentially mixing 1.8 mL of the sample, 0.2 mL of Solution D, 2.0 mL of Solution A, 1.0 mL of Solution B, and 0.2 mL of Solution C in a sealed vial. After thorough shaking, the mixture was allowed to react in the dark for 2 hours before performing UV-Vis measurement at 650 nm.

S1.7 Determination of urea, NO_3^-, NO_2^-

The urease method [9] was employed for the indirect qualitative and quantitative detection of urea in solution, leveraging the specific catalytic activity of urease, which facilitates the hydrolysis of urea into two molecules of NH_3 and one molecule of CO_2. By measuring the difference in ammonia concentration before and after hydrolysis, we can indirectly calculate the corresponding urea concentration. Importantly, the urease method is minimally affected by potential interfering by-products (NO_2^-, NH_3, NH_2OH, and N_2H_4), making it a precise and reliable technique for urea quantification [10].

The detection and quantification of urea in this study were primarily conducted using the urease method, detailed as follows: a 5 $mg \cdot mL^{-1}$ urease solution was prepared by dissolving urease in a 10 $g \cdot L^{-1}$ D buffer solution. A mixture was then prepared by combining 200 μL of the urease solution with 1.8 mL of the post-reaction solution in a color-developing vial. This mixture was incubated in a constant temperature shaker at 37 °C for 40 minutes, after which the ammonia concentration was quantified using the indophenol blue method following cooling to room temperature. The measured

ammonia concentration represents the sum of the original ammonia concentration in the solution and the ammonia produced from urea hydrolysis, which was then substituted into the NH_3 standard curve (Figure S3).

The diacetyl monoxime and liquid chromatography methods were utilized for double-checking: (1) High-performance liquid chromatography (HPLC): The detection conditions and data are presented in Table S3 and Figure S4. (2) Diacetyl monoxime (DAMO) method: The DAMO method was employed as described by Lv et al. [11]. A mixed acid solution was prepared by combining 50 mL of H_3PO_4 (85%), 150 mL of H_2SO_4 (98%), and 300 mL of pure water, followed by cooling. Subsequently, 83.3 mg of $FeCl_3 \cdot 6H_2O$ was added and dissolved to obtain solution A. In a separate preparation, 1.25 g of DAMO and 25 mg of thiourea were dissolved in 250 mL of water, forming solution B. Solutions A and B were kept separate until further use. Sequentially, 6 mL of solution A, 3 mL of solution B, and 3 mL of urea-containing solution were mixed thoroughly and placed in an oil bath at 100°C for 25 minutes. After cooling, the absorbance of the resulting mixture was measured at 525 nm, with data presented in Figure S5.

The concentration of urea and its yield can be calculated, as described by the following equation （S1, S2）:

$$m_{urea} = (m_b - m_a)/2 \quad \text{（S1）}$$

$$R_{\text{urea}} = \frac{C_{\text{urea}} \times V}{\text{t} \times \text{m}_{\text{cat}}} \quad \text{（S2）}$$

where:

m_a and m_b represent the molar mass of NH_3 before and after the decomposition experiment, respectively.

R_{urea}=Urea yield ($\mu mol \cdot h^{-1} \cdot gcat^{-1}$),

C_{urea} = concentration of urea (μg/mL) determined by DAMO method,

V = volume of solution (mL),

t = reaction time (h),

m_{cat} = mass of catalyst used (mg).

Determination of NO_2^- Concentration in Test Solution: Add 0.2 g N-(1-naphthyl)ethylenediamine dihydrochloride, 4 g p-aminobenzenesulfonamide, and 10 mL phosphoric acid to 50 mL deionized water as the color-developing reagent. Then, mix 5 mL of the test liquid with 0.1 mL of the color-developing reagent and shake thoroughly. After 20 minutes, record the absorbance at 540 nm using a UV-visible spectrophotometer to determine the NO_2^- concentration, with data presented in Figure S6a.

Determination of NO_3^- Concentration in Test Solution: Add 1 mL of 1 M HCl to a 50 mL cuvette containing the test solution. Then add 0.1 mL of 0.8 wt.% aminosulfonic acid to eliminate the influence of nitrites. Shake the mixture thoroughly. After 10 minutes, measure the absorbance at wavelengths of 220 nm and 275 nm, respectively. Calculate the absorbance using Equation S3, with data presented in Figure S6b.

$$A_{nitrate-N} = A_{220nm} - 2A_{275nm} \quad (S3)$$

S1.8 The quantum efficiency

In order to evaluate the apparent quantum efficiency (AQE) of Cu/TT, 400 nm wavelength light was used as the light source. The light intensity was tested by a fully automated optical power meter (CEL-NP2000-2(10)A). The AQE values for urea yield were calculated based on the following equation (S4):

$$AQE\ (\%) = 100 \times \frac{[\text{Product formation(mol)}] \times \mathrm{N_A} \times K}{\frac{[\text{total input energy}\ (W)] \times [\text{time}\ (\mathrm{s})]}{h\nu}} \quad (S4)$$

Where:

[Product formation (mol)] is the number of moles of urea produced (1.146×10^{-7} mol);

N_A is Avogadro's constant (6.02×10^3 mol^{-1}). is the transfer of electrons in the reaction (kurea = 6);

h is Plank's constant (6.62×10^{-34} J·s);

[Time (s)] indicates the irradiation time (60 min);

ν is the incident light frequency ($\nu = c/\lambda$, speed of light ($c=3\times10^8$ m/s) and

monochromatic wavelength (=400 nm);

[Total input energy (W)] can be calculated from [incident light intensity (400 nm = 400 mW cm^{-2}) × irradiated area (3.14 cm^{-2})].

S1.9 In-situ infrared spectroscopic measurements

In situ Fourier-transform infrared (FT-IR) spectroscopic analysis was performed using an infrared spectrometer（INVENIO, Bruker Corporation, Germany） equipped with a liquid nitrogen-cooled mercury-cadmium-telluride (MCT) detector and an attenuated total reflection (ATR) liquid-phase cell. A 300 mW/cm^2 xenon lamp (CEL-PE300L-3A, Beijing China) coupled with a quartz optical fiber served as the irradiation source. Prior to catalytic testing, background spectra were acquired under nitrogen purging for30 min in 100 mL of 0.1 M $KHCO_3$/0.1 M KNO_3 electrolyte to establish baseline conditions and eliminate atmospheric contaminants. After pretreatment, CO_2 saturation was achieved through continuous bubbling in the dark, followed by immediate spectral acquisition post-gas flow termination. Photocatalytic reactions were initiated under xenon lamp illumination, with time-resolved infrared spectra recorded at 10-min intervals over a 60-min irradiation period.

S1.10 Computational Details

First-principles density functional theory (DFT) calculations were conducted using the Vienna Ab Initio Package (VASP). The Perdew–Burke–Ernzerhof (PBE) form of the generalized gradient approximation (GGA) was employed to describe exchange-correlation interactions [12]. Projected augmented wave (PAW) potentials were utilized to represent the ionic cores, with valence electrons accounted for by a plane wave cut-off energy of 400 eV [13]. The convergence criteria for the electronic and ionic relaxation were set to 10^{-6} eV and 0.02 eV/Å, respectively. Given the significance of van der Waals interactions in molecular bonding, Grimme's DFT-D3 method for dispersion forces was included [14]. To address the effect of NO_3^- chargedness on the free energy, we used a background charge compensation model with corresponding corrections. The Hubbard U correction was applied to account for the

effect of localized d electrons, with U values set at 4.5 eV for Cu 3d and 3.3 eV for Ti 3d on the transition metal ions. To accurately represent the experimental system, the computational model was constructed as follows: the Ti_3C_2 MXene was modeled using its stable (001) facet, and the major (101) facet of TiO_2 was exposed in the model. The heterojunction interface is modeled by placing the TiO_2 (101) face on the Ti_3C_2 (001) face, and the Cu/TT model was modeled by adding a Cu atom to the TT. In this model, copper is anchored near the Ti_3C_2 interface on the TiO_2 surface (or defect sites) via Cu–O–Ti bonds[15]. A 15 Å vacuum was introduced in the direction perpendicular to the surface for all the models. A 2x2x1 k-point mesh was utilized for all slab model calculations.

S2. Supplementary Figures and Tables

Table S1. The effect of reaction parameters (temperature and time) on urea yield in synthesis using TiO_2/Ti_3C_2 as a catalyst

Sample no.	Sample label	Urea Yield Rate(μmol·h^{-1}·$gcat^{-1}$)
TT1	180/6h	1.92
TT2	180/15h	4.78
TT3	180/24h	3.82
TT4	200/6h	2.67
TT5	200/15h	4.97
TT6	200/24h	4.43
TT7	220/6h	3.42
TT8	220/15h	5.26
TT9	220/24h	4.43

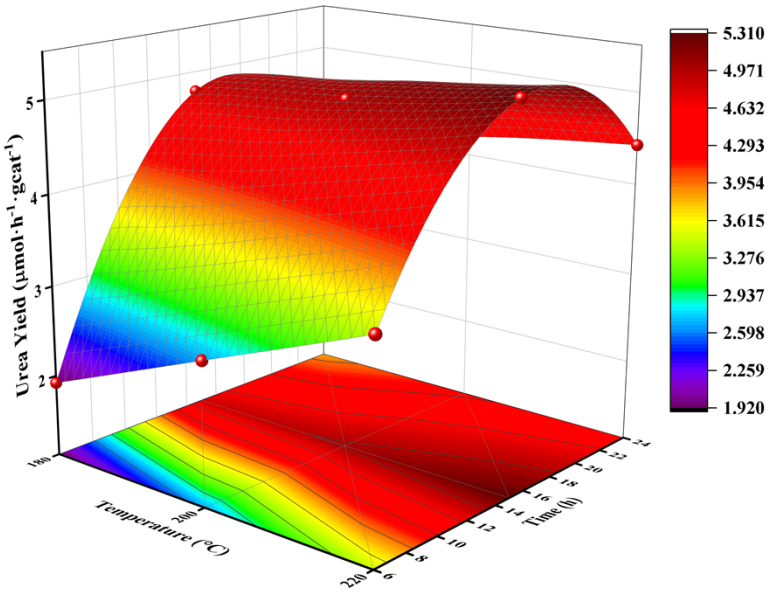

Figure S1. Three-dimensional surface plot of the effects of temperature and synthesis time on urea yield

Table S2. Urea detection conditions.

Sports event	Parametric
chromatographic column	ShimNexUPC18（5 um，4.6×150mm）
detection wavelength	198 nm
column temperature	30 ℃
mobile phase	Acetonitrile: Water(95: 5)
flow rates	1 mL/min
injection volume	10 uL
running time	6.8 min

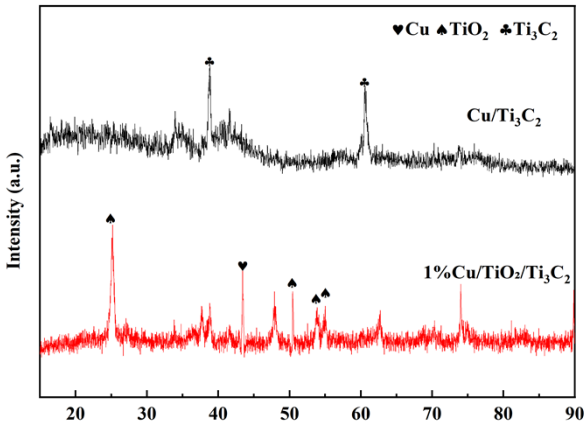

Figure S2. XRD patterns of 1% Cu/TT and Cu/Ti_3C_2. Only the diffraction peaks of Ti_3C_2 were observed in Cu/Ti_3C_2, and the diffraction peaks of Cu and TiO_2 were as shown in the figure of 1% Cu/TT, so that monoatomically dispersed Cu/Ti_3C_2 materials were successfully prepared.

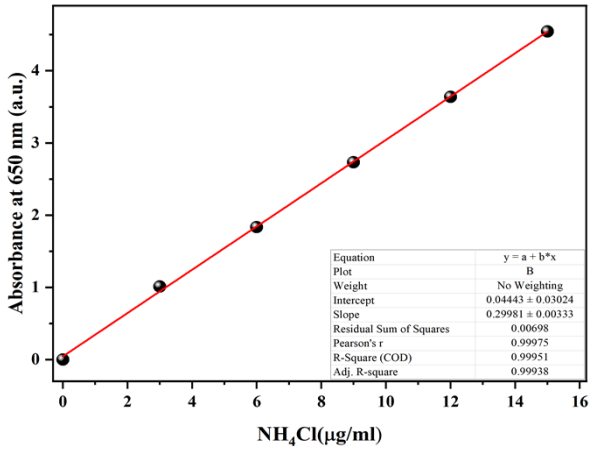

Figure S3. Calibration curve used for estimation of NH_3.

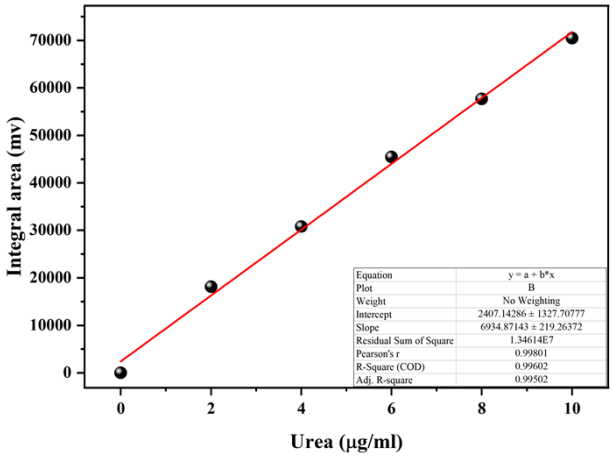

Figure S4. HPLC Standard Curve for Urea Solution.

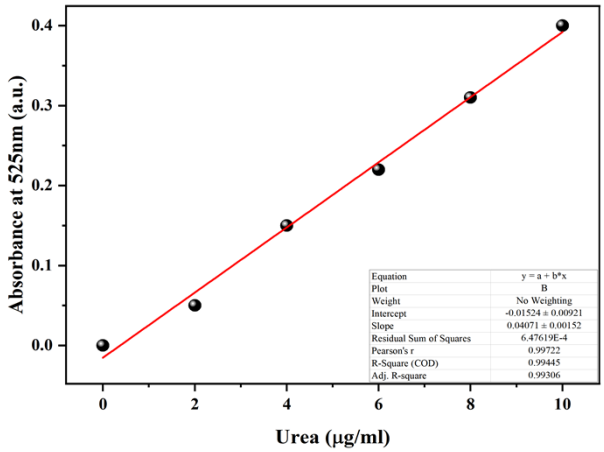

Figure S5. Calibration curve used for estimation of urea.

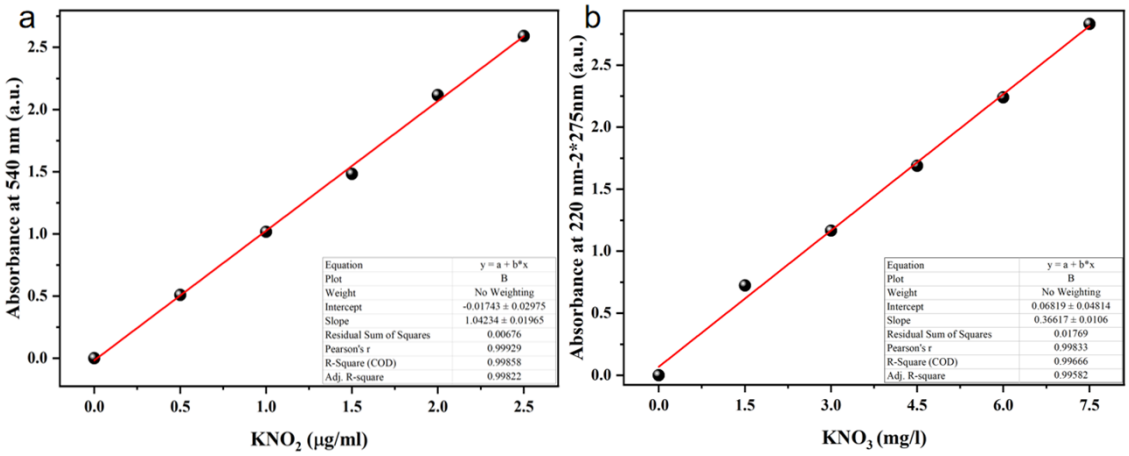

Figure S6. Calibration curve used for estimation of (a) NO_2^- and (b) NO_3^-.

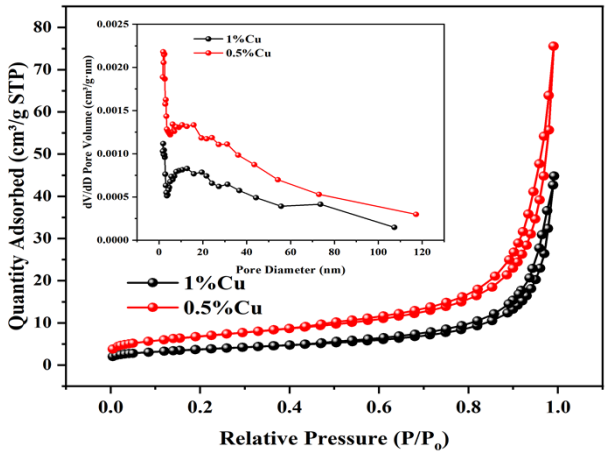

Figure S7. N_2 adsorption-desorption isotherms and pore size distribution of the Cu/TT catalysts with 0.5% and 1% Cu loadings.

Table S3. Textural properties of the Cu/TT catalysts derived from N_2 physisorption.

Catalyst	BET Surface Area (m^2/g)	Total Pore Volume (cm^3/g)	Average Pore Size (nm)
0.5%Cu/TT	23.4892	0.1151	19.6070
1%Cu/TT	12.8360	0.0671	20.9357

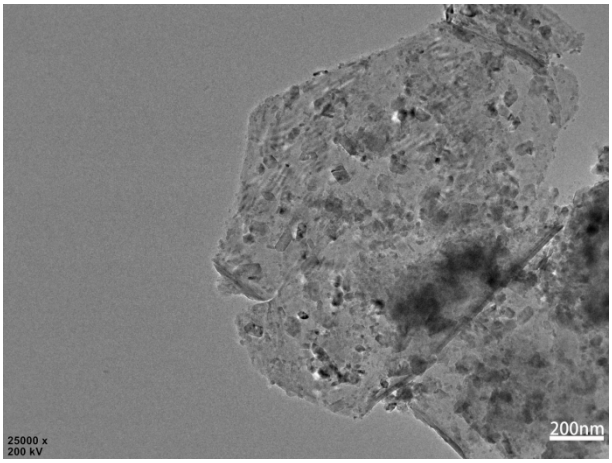

Figure S8. TEM image of 0.5% Cu/TT.

Table S4. Quantitative EDS analysis of Cu distribution from HAADF-STEM on Cu/TT catalyst.

Analysis Region	Size (nm^2)	Cu Mass% (Wt.%)	Cu Atom% (At.%)
Region 1	10^6	0.49	0.34
Region 2	10^6	0.73	0.48
Region 3	10^6	0.94	0.63
Mean ± SD	-	0.72±0.23	0.48±0.15
Relative Standard Deviation (RSD)		31.9%	31.3%

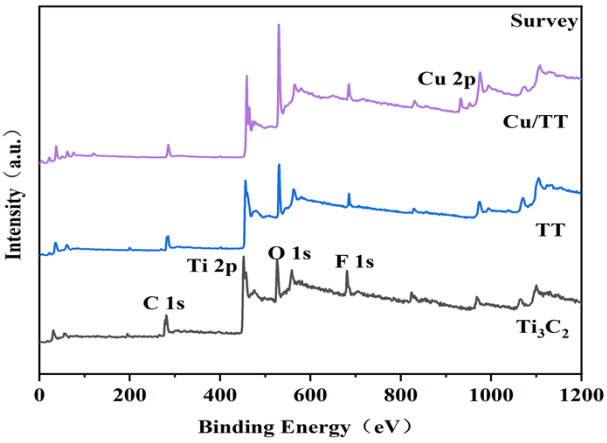

Figure S9. The Survey XPS spectra of Ti_3C_2, TT, and Cu/TT.

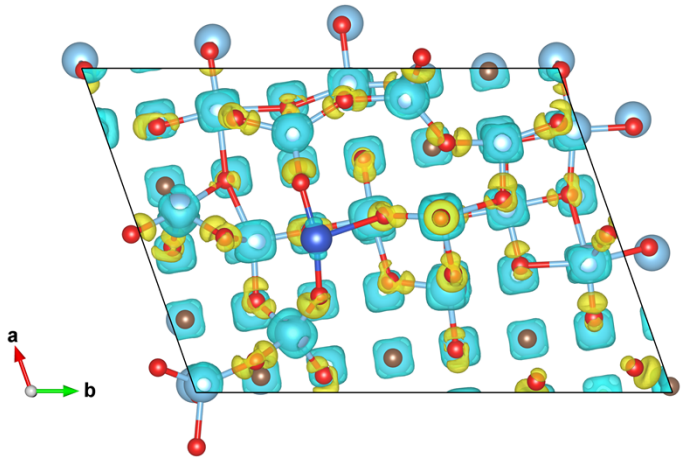

Figure S10. Charge Density Difference Visualizing Electron Transfer through the Cu-O-Ti Bridge.

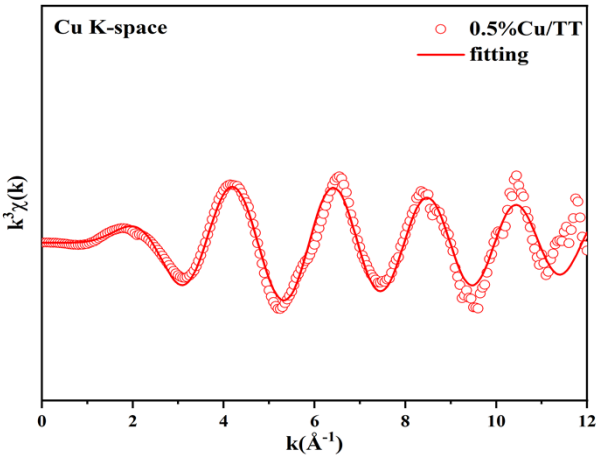

Figure S11. The fitting images for Cu K-edge EXAFS spectra in R-space of Cu/TT.

Table S5. Batch-to-batch reproducibility test for the synthesis of 0.5% Cu/TT catalyst.

Batch No.	Urea Yield (μmol·h^{-1}·$gcat^{-1}$)	Mean±Standard Deviation (SD)	Relative Standard Deviation (RSD)
1	11.57		
2	11.42	11.57 ± 0.15	1.3%
3	11.71		

Table S6.Photocatalytic performance parameters with standard deviations (mean ± SD, n = 3).

Catalyst	Description	Urea Yield (μmol·h^{-1}·$gcat^{-1}$)	Selectivity (%)	(AQE) at 400 nm (%)
Cu/TT	Target catalyst	11.57±0.37	64.78±2.1	0.88±0.03
TT	TiO_2/Ti_3C_2 support (no Cu)	5.26±0.16	48.6±3.5	0.4±0.022
Cu/Ti_3C_2	Cu loaded on Ti_3C_2	6.25±0.31	43.59±2.6	0.475±0.032
0.25% Cu/TT	Low Cu loading	9.41±0.38	61.49±2.9	0.716±0.044
1% Cu/TT	High Cu loading	6.1±0.21	55.34±2.2	0.464±0.027

Table S7. Comparison of urea yield (mean ± SD, n = 3) over Cu/TT and benchmark catalysts.

Catalyst	Description	Urea Yield (μmol·h^{-1}·$gcat^{-1}$)
Cu/TT	Target catalyst (0.5 wt% Cu on TiO_2/Ti_3C_2)	11.57±0.37
TiO_2	Pristine TiO_2 nanoparticles	2.92±0.21
Ti_3C_2	Bare Ti_3C_2 MXene	1.74±0.18
$Cu/TiO_2 + Ti_3C_2$	Physical mixture of Cu-loaded TiO_2 (0.5 wt%) and Ti_3C_2	7.29±0.29

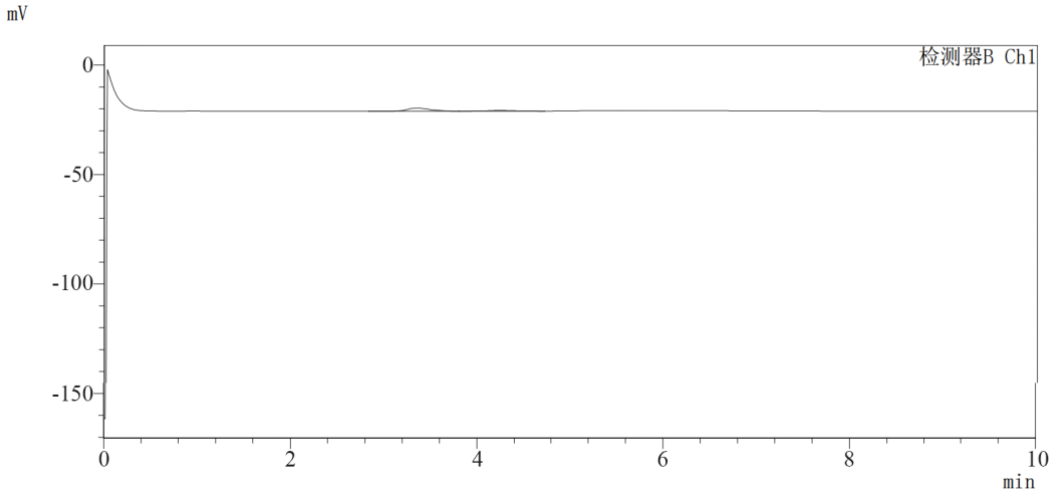

Figure S12. Liquid chromatogram of the stringent blank control experiment.

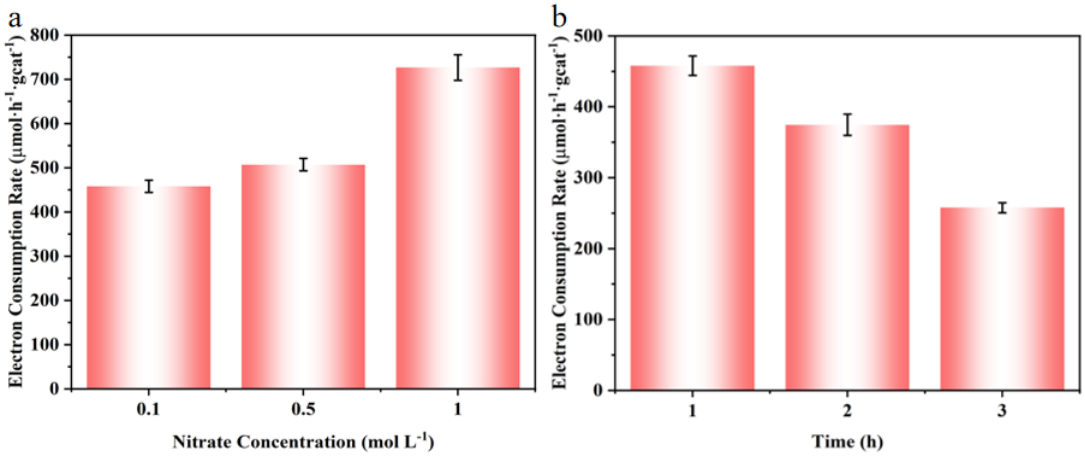

Figure S13. Calculated electron consumption rate of Cu/TT with different nitrate concentration (a) and different reaction duration (b). Electron consumption rate = total electron consumption / (catalyst mass * time), while total electron consumption = hourly urea production (mol/L) * 8e^-/mol.

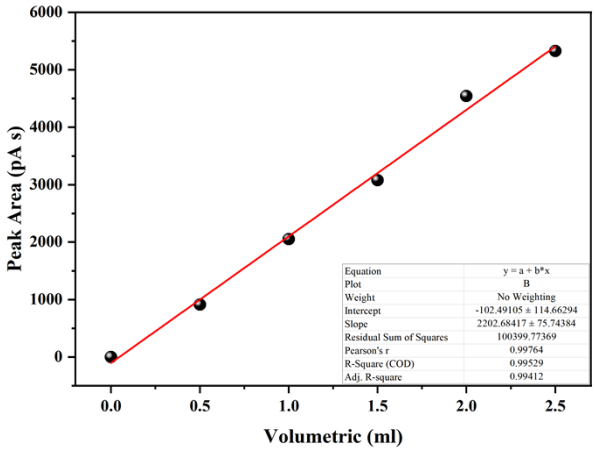

Figure S14. Calibration curve used for estimation of CO.

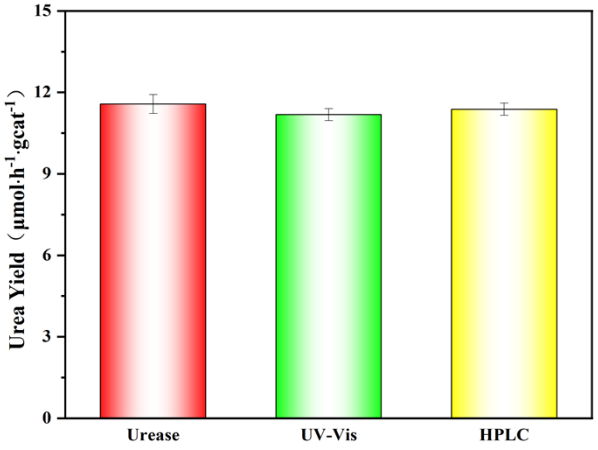

Figure S15. Comparison of Urea Yields Among Three Methods.

Table S8. Comparison of experimental data of photocatalytic nitrogen fixation for urea Production.

System/Conditions	Catalyst	Urea Yield Rate	AQE(%)	Light Intensity(mW cm^{-2})	Reference
N_2: CO_2（1：1）	CeO_2	6.46 μmol·h^{-1}·$gcat^{-1}$	0.013 (420 nm)	500	[16]
N_2: CO_2（1：1）	Cu SA-TiO_2	7.20 μmol·h^{-1}·$gcat^{-1}$			[17]
N_2: CO_2（1：1）	Pd-CeO_2	9.20 μmol·h^{-1}·$gcat^{-1}$		500	[18]
N_2: CO_2（1：1）	Ni_1-CdS/WO_3	10.4 μmol·h^{-1}·$gcat^{-1}$	0.15 (385 nm)	100	[19]

N_2：CO_2（1：1）	JH Fe/Co@TiO_2	10.64 μmol·h^{-1}·$gcat^{-1}$	0.33 (365 nm)	100	[20]
5 mM NO_3^-+CO_2	CCBT-Ar	0.00372 μmol·h^{-1}·$gcat^{-1}$	0.022 (405 nm)		[21]
0.1 M NO_3^-+CO_2	at.-Pd@TiO_2/Gr	3.2 μmol·h^{-1}·$gcat^{-1}$	1.05 (400 nm)	4.4	[22]
0.1 M NO_3^-+CO_2	Cu/TiO_2/Ti_3C_2	11.57 μmol·h^{-1}·$gcat^{-1}$	0.88 (400 nm)	400	This work

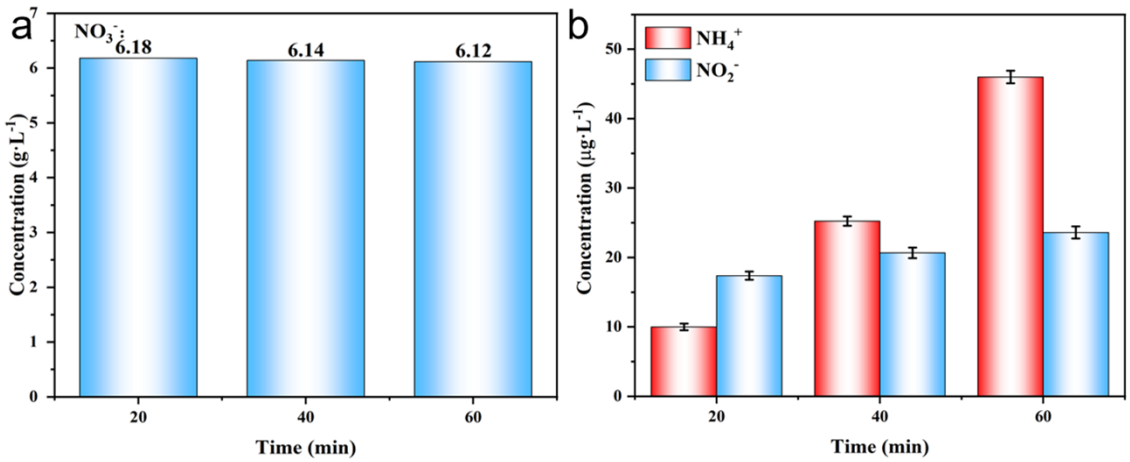

Figure S16. Concentrations of (a) NO_3^- and (b) NO_2^- and NH_4^+at different reaction times.

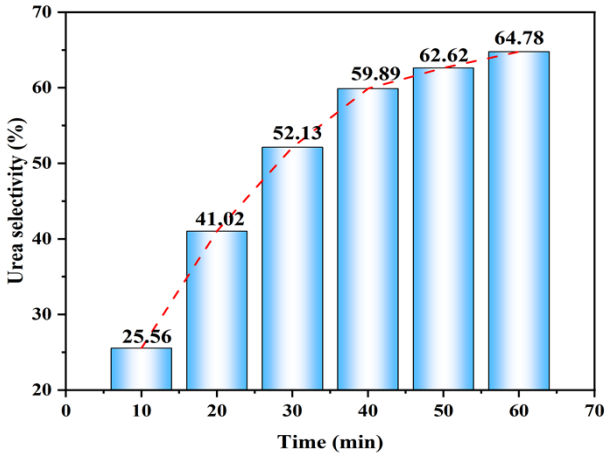

Figure S17. Time-dependent urea selectivity over the Cu/TT catalyst.

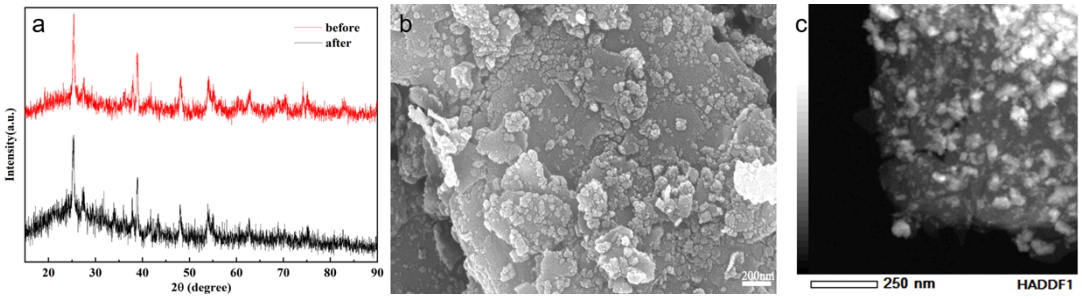

Figure S18. (a) XRD patterns of Cu/TT before and after cycling, (b) SEM images and (c) HAADF-STEM of Cu/TT after cycling.

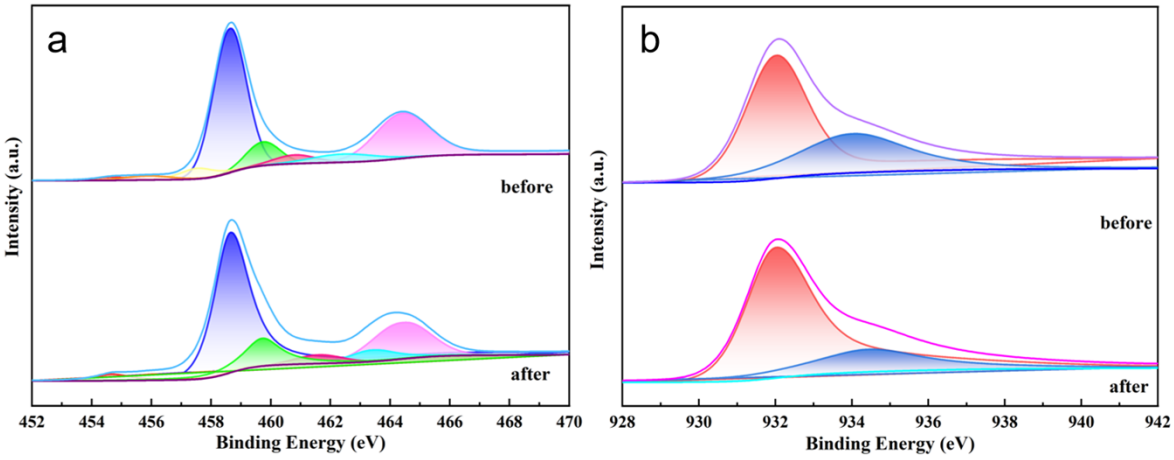

Figure S19. XPS spectra of (a) Ti and (b) Cu before and after cycling.

Table S9. EIS fitting table for the resulting catalyst in 0.1 M NO_3^- saturated CO_2.

Sample	R_{ct}(ohm)	R_h(ohm)
0.5% Cu/TT	398	503
0.25% Cu/TT	573	2320
1% Cu/TT	751	34781
TT	1437	141401

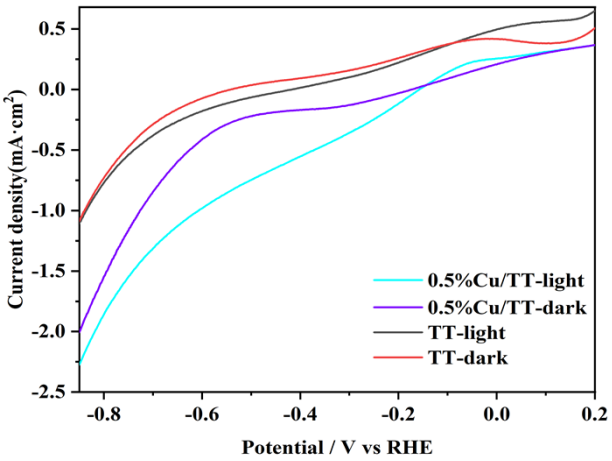

Figure S20. Comparison of LSV curves of samples.

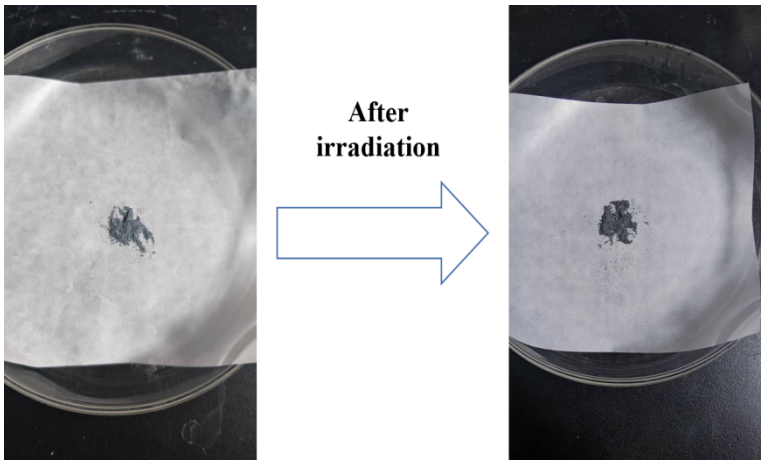

Figure S21. Color change of 5% Cu/TT photocatalyst powder before and after irradiation.

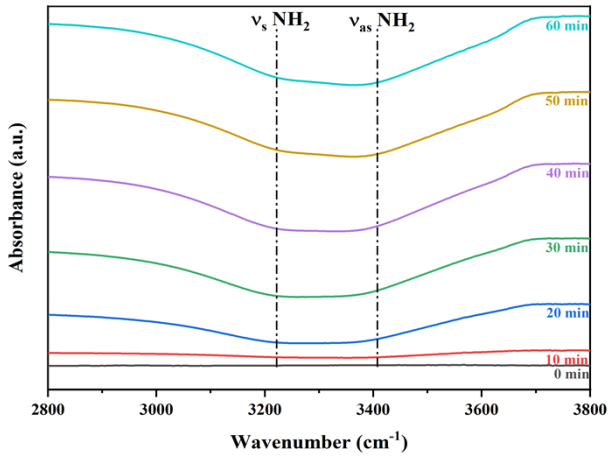

Figure S22. Infrared signals in the range 2800 to 3800 cm^{-1}.

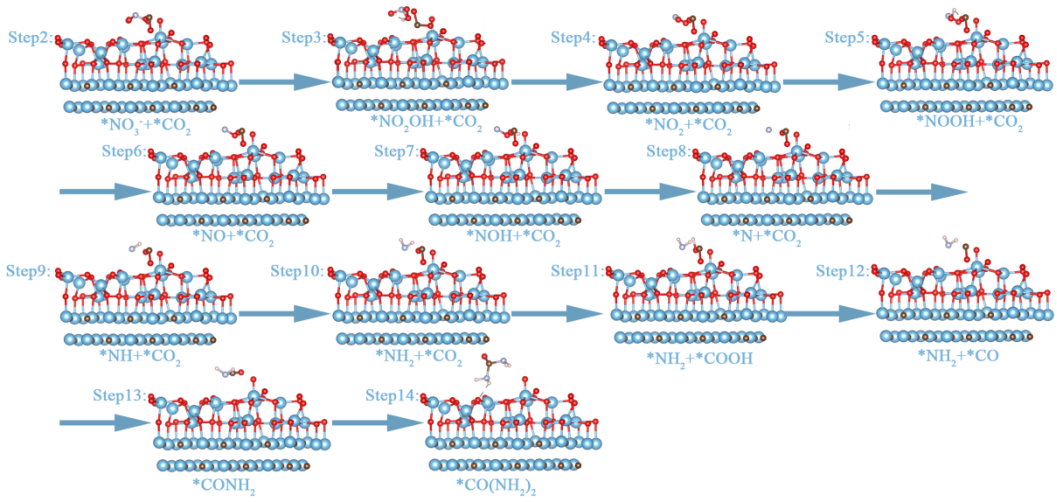

Figure S23.Optimized intermediate structures in the pathway for urea synthesis on TT. The silver, beige, black, indigo and red spheres represent N, H, C, Ti and O atoms, respectively.

References

[1] Zou, X.; Zhao, X.; Zhang, J.; Lv, W.; Qiu, L.; Zhang, Z. Photocatalytic degradation of ranitidine and reduction of nitrosamine dimethylamine formation potential over MXene–Ti_3C_2/MoS_2 under visible light irradiation. J. Hazard. Mater. 2021, 413, 125424.

[2] Bao, Y.; Pan, J.; Wu, H.; Zhang, Z.; Li, Y.; Wang, Z.; Hui, T.; Yang, B.; Li, J.; Hu, H.; Jiang, J.; Liu, J. Designed 2D/2D/2D $Bi_2WO_6/Ti_3C_2/SnNb_2O_6$ Z-scheme heterojunction via interfacial chemical bond with enhanced photocatalytic activity. J. Alloys Compd. 2023, 948, 169762.

[3] Isac, L.; Cazan, C.; Andronic, L.; Enesca, A. CuS-based nanostructures as catalysts for organic pollutants photodegradation. Catalysts 2022, 12, 1135.

[4] Fu, X.; Kong, Y.; Wang, M.; Cai, T.; Zeng, Q. MXene derived Ti_3C_2/TiO_2/Ag persistent photocatalyst with enhanced electron storage capacity for round-the-clock degradation of organic pollutant. J. Colloid Interface Sci. 2024, 656, 233-240.

[5] Liu, A.; Liang, X.; Yang, Q.; Ren, X.; Gao, M.; Yang, Y.; Ma, T. Electrocatalytic synthesis of ammonia using a 2D Ti_3C_2 MXene loaded with copper nanoparticles. ChemPlusChem 2021, 86, 166–170.

[6] J. Zhang, Z. Zhou, Z. Feng, H. Zhao, G. Zhao, Fast generation of hydroxyl radicals by rerouting the electron transfer pathway via constructed chemical channels during the photo-electro-reduction of oxygen, Environ. Sci. Technol. 56 (2022) 1331–1340.

[7] L. Yuan, S. Hung, Z. Tang, H. Chen, Y. Xiong, Y. Xu, Dynamic evolution of atomically dispersed cu species for CO2 photoreduction to solar fuels, ACS, Catalysis 9 (2019) 4824–4833.

[8] Searle, P. L. The Berthelot or indophenol reaction and its use in the analytical chemistry of nitrogen. A review. Analyst. 1984, 109, 549-568.

[9] Feng, Y.; Yang, H.; Zhang, Y.; Huang, X.; Li, L.; Cheng, T.; Shao, Q. Te-doped Pd nanocrystal for electrochemical urea production by efficiently coupling carbon dioxide reduction with nitrite reduction. Nano Lett. 2020, 20, 8282-8289.

[10] Wei, X.; Wen, X.; Liu, Y.; Chen, C.; Xie, C.; Wang, D.; Wang, S. Oxygen vacancy-mediated selective C–N coupling toward electrocatalytic urea synthesis. J. Am. Chem. Soc. 2022, 144, 11530-11535.

[11] Lv, C.; Zhong, L.; Yan, C.; Chen, M.; Lee, C.; Liu, D.; Li, S.; Liu, J.; Yan, Q.; Liu, H.; Song, L.; Fang, Z.; Yu, G.; Kong, Y.; Chen, G. Selective electrocatalytic synthesis of urea with nitrate and carbon dioxide. Nat. Sustain. 2021, 4, 868-876.

[12] Deng, Y.; Guo, Y.; Jia, Z.; Liu, J. C.; Guo, J.; Cai, X.; Dong, C.; Wang, M.; Li, C.; Diao, J.; Jiang, Z.; Xie, J.; Wang, N.; Xiao, H.; Xu, B.; Zhang, H.; Liu, H.; Li, J.; Ma, D. Few-atom Pt ensembles enable efficient catalytic cyclohexane dehydrogenation for hydrogen production. J. Am. Chem. Soc. 2022, 8, 3535-3542.

[13] Chu, K.; Liu, Y.; Li, Y.; Guo, Y.; Tian, Y.; Zhang, H. Multi-functional Mo-doping in MnO_2 nanoflowers toward efficient and robust electrocatalytic nitrogen fixation. Appl. Catal. B Environ. 2020, 264, 118525.

[14] Ye, J.; Liu, C.; Mei, D.; Ge, Q. Active oxygen vacancy site for methanol synthesis from CO_2 hydrogenation on In_2O_3 (110): A DFT study. ACS Catal. 2013, 3, 1296−1306.

[15] Hui, D.; Li, S.; Wu, D.; Liu, L.; Li, S.; Wang, S.; Liu, H.; Zhang, X.; Li, B. Microstructure and properties of Cu–Ti matrix composites with in situ dispersive oxide fabricated by internal oxidation process. J. Mater. Sci. 2025, 60, 5977-5995.

[16] Yang, S.; Zhang, W.; Pan, G.; Chen, J.; Deng, J.; Chen, K.; Niu, L. Photocatalytic Co-reduction of N_2 and CO_2 with CeO_2 catalyst for urea synthesis. Angew. Chem. Int. Ed. 2023, 135, e202312076.

[17] Li, D.; Zhao, Y.; Miao, Y.; Zhou, C.; Zhang, L. P.; Wu, L. Z.; Zhang, T. Accelerating electron-transfer dynamics by TiO_2-immobilized reversible single-atom copper for enhanced artificial photosynthesis of urea. Adv. Mater. 2022, 34, 2207793.

[18] Yang, S.; Deng, J.; Chen, J.; Tan, Q.; Liu, T.; Chen, K.; Niu, L. Photocatalytic C–N coupling towards urea synthesis with a palladium-supported CeO_2 catalyst. Catal. Sci. Technol. 2023, 13, 1855−1865.

[19] Zhang, Y.; Sun, Y.; Wang, Q.; Zhuang, Z.; Ma, Z.; Liu, L.; Zheng, X. Synergy of photogenerated electrons and holes toward efficient photocatalytic urea synthesis from CO_2 and N_2. Angew. Chem. Int. Ed. 2024, 136, e202405637.

[20]]Yang, H.; Li, T.; Li, Z.; Huang, K.; Zhang, Z.; Meng, X. Dual-metal regulation of PCET and spin polarization synergism for efficient photocatalytic urea synthesis. Chem. Eng. J. 2025, 167328.

[21] Sun, H.; Lin, Z.; Tang, R.; Liang, Y.; Zou, S.; Zhang, X.; Huang, J. Enhanced solar urea synthesis from CO_2 and nitrate waste via oxygen vacancy mediated-TiO_x support lead-free perovskite. Appl. Catal. B Environ. 2025, 360, 124511.

[22] Hu, W. Y.; Li, Q. Y.; Xu, D.; Gao, P.; Qiao, P. Z.; Li, D.; Li, X. H. Integrating Pd (I) atoms in schottky junctions for visible-light-driven urea production from ambient nitrogenous species and CO_2. CCS Chemistry 2024, 6, 3008-3017.